Journal of Insect Physiology 130 (2021) 104199

Contents lists available at ScienceDirect

Journal of Insect Physiology

journal homepage: www.elsevier.com/locate/jinsphys

Using μCT in live larvae of a large wood-boring beetle to study tracheal oxygen supply during development

Philipp Lehmann [a,b,*], Marion Javal [a], Anton Du Plessis [c], John S. Terblanche [a]

[a] Centre for Invasion Biology, Department of Conservation Ecology and Entomology, Stellenbosch University, Stellenbosch, South Africa
[b] Department of Zoology, Stockholm University, Sweden
[c] CT Scanner Facility, Central Analytical Facilities, Stellenbosch University, Stellenbosch, South Africa

ARTICLE INFO

Keywords:
Gas exchange
Trachea
μCT
Pest insect
Coleoptera
Methodology

ABSTRACT

How respiratory structures vary with, or are constrained by, an animal's environment is of central importance to diverse evolutionary and comparative physiology hypotheses. To date, quantifying insect respiratory structures and their variation has remained challenging due to their microscopic size, hence only a handful of species have been examined. Several methods for imaging insect respiratory systems are available, in many cases however, the analytical process is lethal, destructive, time consuming and labour intensive. Here, we explore and test a different approach to measuring tracheal volume using X-ray micro-tomography (μCT) scanning (at 15 μm resolution) on living, sedated larvae of the cerambycid beetle *Cacosceles newmannii* across a range of body sizes at two points in development. We provide novel data on resistance of the larvae to the radiation dose absorbed during μCT scanning, repeatability of imaging analyses both within and between time-points and, structural tracheal trait differences provided by different image segmentation methods. By comparing how tracheal dimension (reflecting metabolic supply) and basal metabolic rate (reflecting metabolic demand) increase with mass, we show that tracheal oxygen supply capacity increases during development at a comparable, or even higher rate than metabolic demand. Given that abundant gas delivery capacity in the insect respiratory system may be costly (due to e.g. oxygen toxicity or space restrictions), there are probably balancing factors requiring such a capacity that are not linked to direct tissue oxygen demand and that have not been thoroughly elucidated to date, including CO_2 efflux. Our study provides methodological insights and novel biological data on key issues in rapidly quantifying insect respiratory anatomy on live insects.

1. Introduction

What determines the metabolic scope of animals? One important aspect is the delivery capacity of the oxygen supply system. In insects, oxygen is supplied through air-filled tubes called tracheae (Chapman, 2012; Harrison et al., 2012). These originate in ventilatory valves embedded in the cuticle, called spiracles, that lead to a branching network of tubes of decreasing diameter that ultimately end in close proximity to the tissues and cells to which they supply oxygen. The smallest tracheae, with a diameter smaller than ~2 μm, are called tracheoles and the major site of oxygen exchange (Schmitz and Perry, 1999; Wigglesworth, 1983).

As insects grow, their body mass increases exponentially and as tissue is being added, it is expected that the cost of maintaining these tissues, reflected in the resting metabolic rate (rmr), increases as well (Greenlee and Harrison, 2005; Kivelä et al., 2016). To increase oxygen supply, insects replace the larger components of the tracheal air supply system during moulting (Callier and Nijhout, 2011) and also show increases in smaller tracheal structures during the inter-moult period of growth (Helm and Davidowitz, 2013; Wigglesworth, 1954). Still, how well the overall size of the oxygen supply system matches tissue growth in developing insects remains surprisingly unclear (Callier and Nijhout, 2011; Snelling et al., 2011a). Strongly matched growth of structures linked to oxygen demand (metabolically active tissues) and supply (tracheal system) was proposed within the framework of symmorphosis (Weibel et al., 1991). The theory suggests that excess functional capacity of tissues in a supply-demand network should be selected against over evolutionary timescales, as tissues, especially neural, muscle and gut, are energetically costly (Niven and Laughlin, 2008).

Studies of metabolic supply have used several methods to estimate

* Corresponding author at: Department of Zoology, Stockholm University, 10691 Stockholm, Sweden.
E-mail address: philipp.lehmann@zoologi.su.se (P. Lehmann).

https://doi.org/10.1016/j.jinsphys.2021.104199
Received 5 November 2020; Received in revised form 15 January 2021; Accepted 1 February 2021
Available online 5 February 2021

tracheal capacity. These have included light microscopy (Miller, 1966; Wigglesworth, 1930; Snelling et al., 2011b), volume displacement measures (Helm and Davidowitz, 2013), confocal microscopy (Harrison et al., 2018a) and electron microscopy (Snelling et al., 2011c). Lately X-ray micro-tomography (μCT) has become an additional tool with which to study tracheal networks (Aitkenhead et al., 2020; Alba-Tercedor et al., 2019; Greenlee et al., 2009; Harrison et al., 2018a; Javal et al., 2019; Raś et al., 2018; Shaha et al., 2013; Wasserthal et al., 2018). Using μCT has the benefit of allowing reconstruction of the intact tracheal tree in its three-dimensional configuration. However, previous studies have typically made use of dead animals, sometimes frozen or histologically fixed, which can have significant impact on details (e.g. collapse, or systemic fluid filling) of tracheal structures (Iwan et al., 2015).

Here we investigate tracheal growth using X-ray micro-tomography (μCT), but perhaps somewhat unusually, we do so using living, sedated larvae of a large-bodied beetle, *Cacosceles newmannii*. We use the method to quantity volume and area of isolated tracheal trees (to a resolution of 15 μm) and compare the relationship between these traits and body mass at two time-points. We also quantify resting metabolic rate across a body mass range, to gain further insight into how metabolic demand varies across ontogeny. Even though this comparison is not the primary purpose of the current investigation, strong matching in traits reflecting both metabolic demand (metabolic rate and body mass) and oxygen supply (tracheal size) would lend support the notion of metabolic symmorphosis. Poor matching would suggest a metabolic demand-supply mismatch to be present during growth in the larvae. The method developed in the present study could prove useful in future studies that rigorously test the scaling relationship between metabolic demand and supply using a large size gradient, especially if insect larvae prove to possess similarly high radio resistance as shown in Lepidopteran pupae previously (Lowe et al., 2013), which would allow designing longitudinal experiments tracking the fitness or performance consequences of a particular structure as it changes over time within the same individual during ontogeny.

2. Materials and methods

2.1. Study animals and rearing conditions

The longhorned beetle *Cacosceles newmannii* (Coleoptera: Cerambycidae) Thomson 1877, is native to South Africa, Mozambique and eSwatini (Ferreira, 1980). For this study we used larvae collected by hand from KwaZulu-Natal sugarcane farms (South Africa, Entumeni district). These were kept individually at 25 °C in a 16L:8D regime, in 30 ml jars containing sterilized peat and *ad libitum* food provision (bits of 10 cm fresh sugarcane stalk). Two opportunistic rounds of μCT measurements were performed, the first 20.4.2018, and the second the 22.6.2018. Three groups of larvae were used, hereafter called A) 8 individuals that were used in both rounds of μCT, B) 6 individuals used only in the second round of μCT, and C) 6 individuals never exposed to μCT, but otherwise maintained similarly. Change in body mass (to 0.1 mg, Mettler Toledo MS104S/01, Switzerland) between the first and second μCT exposure in the A group was compared against change in body mass in the B + C groups (range 9 – 64 days, median 49 days), in order to assess effects of the absorbed radiation dose on growth. No larva moulted during the rearing period, and thus all growth is assumed to represent within-instar growth. Initial body masses were overlapping in the A) individuals 1.4 – 7.5 g, mean 4.3 ± 0.6 g and the B + C) individuals 1.1 – 9.2 g, mean 4.6 ± 0.4 g, and both groups contained all three presumed instars (i.e. instars four to six).

2.2. Respirometry

Before the first μCT scanning larvae were weighed (to the nearest 0.1 mg) and placed individually in a flow-through chamber to measure carbon dioxide production as described previously (Boardman and Terblanche, 2015; Smit et al., 2021). Air flow was regulated at 200 ml min^{-1} (STPD, controlled by a mass flow control valve (Sidetrak, Sierra International, USA)) into a calibrated Li-7000 infra-red CO_2/H2O analyser and standard LiCor software (LiCor, Lincoln, NE, USA). The CO_2 production was recorded differentially (VCO_2) in ppm using a sampling rate of 1 Hz. Measurements were performed in the dark to suppress movement, which was monitored with an infra-red activity detector (AD-2, Sable Systems International, Las Vegas, NV, USA). Insects were given a 5 min equilibration period at 25 °C, after which metabolic rate was measured for 20 to 40 min, ensuring that we captured at least 15 min where animals were immobile (as seen through the activity trace). While inactive the larvae generally showed discontinuous gas exchange (Matthews et al., 2012). Mean CO_2 production was calculated across at least three consecutive discontinuous gas exchange cycles (see Smit et al., 2021). Temperature in the chamber was controlled with a programmable circulating refrigeration and heating water bath (CC410wl, Huber, Berching, Germany). Baseline recordings were taken before and after each run to correct for potential analyser drift, which was typically negligible. Respirometry files were converted from ppm to ml CO_2 $hour^{-1}$ and extracted using Expedata (version 1.9.10, Sable Systems). In order to estimate the scaling of CO_2 production across a larger size gradient, the dataset was merged with that of Smit (Smit et al., 2021), collected in parallel using a similar setup. Since that study measured CO_2 production at 20 and 30 °C we converted all VCO_2 values to 25 °C assuming a temperature coefficient of 2.0 to allow comparisons between the studies. Together, the respirometry dataset contained 34 individuals with body masses ranging from 0.6 to 5.3 g.

2.3. X-ray micro-tomography

X-ray micro-tomography (μCT) was performed with scan parameters optimized as demonstrated previously (du Plessis et al., 2017). In order to obtain high-quality μCT scans we anesthetized larvae with sevoflurane (Sojourn, Piramal, Bethlehem, USA) in accordance with recommendations for insects (MacMillan et al., 2017). We opted for sevoflurane over sedation using CO_2 and cooling, the two most commonly used alternatives, for several reasons. Most importantly, both cooling and CO_2 sedation have been shown to influence growth and long-term fitness of animals, unlike sevoflurane, which in *D. melanogaster* led to no measurable negative effects on treated animals (MacMillan et al., 2017). Further, cooling the scanning chamber sufficiently is challenging due to space limitations and potential interference between heat-exchangers and electronic equipment in the scanner. Thus, sevoflurane-induced anaesthesia is an exciting alternative that we tested here in a new setting. Larvae were placed in 15 ml Falcon tubes surrounded by cotton, upon which 100 – 200 μl of sevoflurane was pipetted. Scans were performed when larvae stopped all movement, in general within 5 – 10 min after the application of the anaesthetic. Before scanning, a wedge of firm closed-cell foam mounting material was inserted along the back of the larva to firmly keep it in place. Both the foam and cotton are of very low density and easy to separate during subsequent segmentation analyses, and an important consideration when designing μCT experiments on live samples. After the scan larvae were immediately returned to holding jars and in each case recovered fully, i.e. started moving, within 60 s upon removal from the sevoflurane-containing Falcon tube.

All samples were scanned (in Falcon tubes) in a General Electric VTomex L240 (General Electric Sensing and Inspection Technologies/Phoenix X-ray, Wunstorff, Germany) μCT-scanner at the CT Scanner Facility at Stellenbosch University, South Africa. Settings were 120 kV and 100 μA for X-ray generation, magnification was set to achieve a voxel size of 15 μm. The size of the larvae limited the lowest possible resolution. At 15 μm voxel size, the head of the largest specimen in the batch could be covered with sufficient field of view to cover two segments of the larva. This voxel size was achieved with a source-detector distance of 600 mm and a source-object distance of 45 mm. Each image

was acquired in 250 ms, with averaging of two images at each rotational step position to enhance image quality. A total of 1500 step positions were used in one full rotation of the sample. Importantly, these settings allowed us to perform scans of approximately 18 min (which is relatively short for μCT), to minimize the time animals spent under sevoflurane anaesthesia.

2.4. Image segmentation and analysis

Image segmentation was performed in Volume Graphics VGSTUDIO MAX 3.2. The process aimed at obtaining a region of interest of the air space inside single tracheal trees for each specimen. We scanned the anterior part of the specimen, including the first 3 spiracular openings. For tracheal nomenclature and abbreviations we follow (Raś et al., 2018) and for analyses, we only considered the tracheal tree branching in from the first metathoracic spiracle (ts_2). Trees on each side of the larva were considered as replicates for the same specimen. Thus we analyzed two trees per individual larva, and took averages from these two trees for the statistical analyses and figures. A surface determination function was applied to identify the material-air interface – this is equivalent to a global thresholding segmentation but uses a local refinement for sub-voxel edge determination. Following this, the next step was to manually close the tracheal entrances (i.e. all spiracles) using the 3D drawing tool provided by the software. The inner air space of the whole tracheal system was then selected using a region growing tool within this closed area (Fig. 1A). The next step was to separate the tracheal tree of interest from the rest of the tracheal system, by manually cutting tracheae connecting other spiracles using the drawing tool. In order to standardize the way a tree was isolated from the rest of the system, several landmarks were chosen. First, the dorsal (dlt) and ventral (vlt) longitudinal tracheal trunks on the anterior end of the ts_2 spiracle were cut halfway towards the mesothoracic spiracle (ts_1) at a characteristic enlargement visible in each specimen (see Fig. 1B). Then, dlt and vlt on the posterior end of the ts_2 spiracle were cut just after the atrium. Finally, the dorsal (dc) and ventral (vc) transversal commissures were cut as close as possible to the atrium of the ts2 spiracle (Fig. 1B). Once a tracheal tree was isolated (i.e. the metathoracic spiracular opening and all trachea attached to that spiracle), its area and volume were extracted in mm^2 and mm^3, respectively (Fig. 1C). Default 3x3x3 median filtering was employed to de-noise images.

The segmented data was saved as an image stack, which was imported in Avizo Fire 9.5.0. The data was further smoothed using a median filter, followed by interactive thresholding to obtain a binarized data set. An auto-skeletonize function was applied (with smoothing 10 and iterations 10). The spatial graph statistics allowed the export of data about the pore skeleton network including all curved segment lengths which could be added together to obtain the total segment length, and statistical information about the mean diameters of all segments were obtained (Fig. 1D). The surface area of a single tracheal tree, associated with a single spiracular opening, was then calculated using the formula:

$$\text{Area of a single tracheal tree} = \sum_{i=1}^{n}(2\pi r_i h_i) \quad (1)$$

where i reflects a particular segment in the tree, π is the pi constant, r_i is the mean radius of that segment, and h_i is its length. Thus we performed and compare two methods of estimating tracheal tree area, one which allows uneven surface determination, and one which assumes trachea

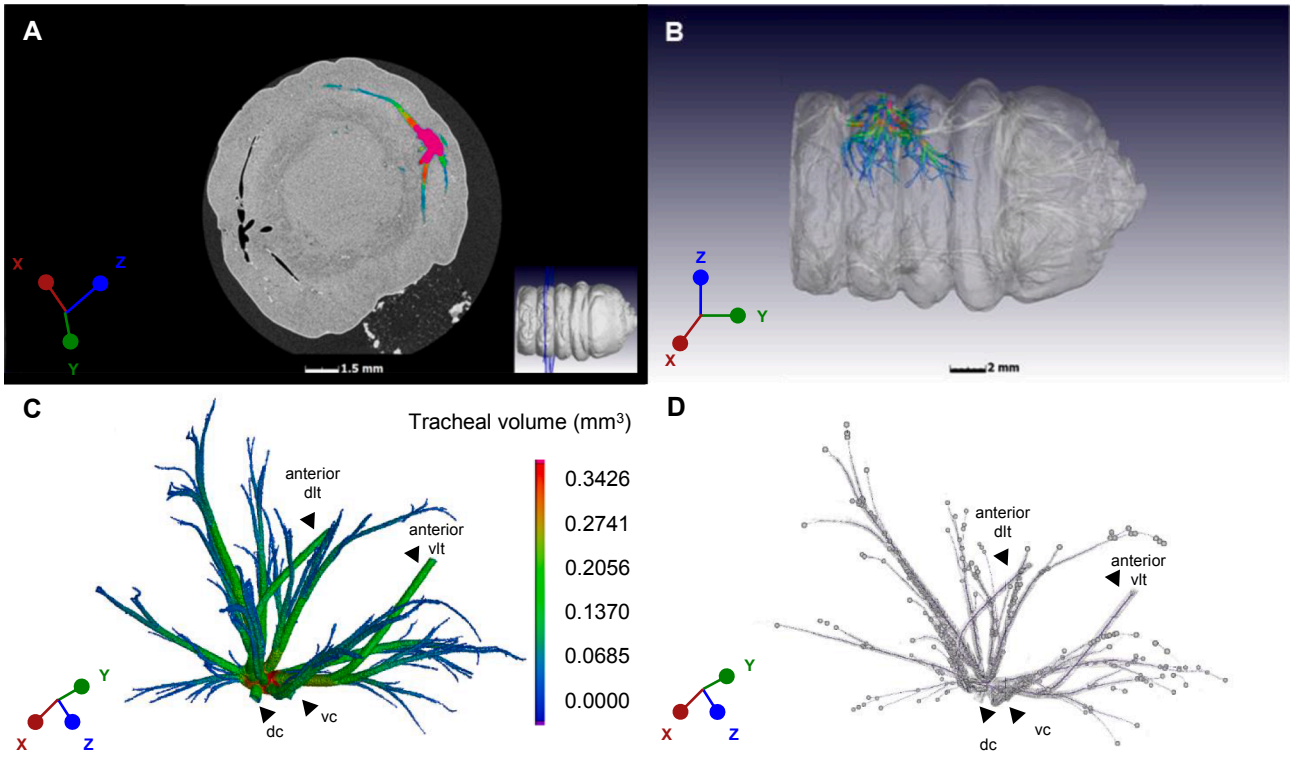

Fig. 1. Example X-ray micro-tomography (μCT) images of larvae of the beetle *Cacosceles newmannii*. Panel (A) shows a 2D slice with single tracheal system highlighted with colors reflecting volumetric rendering, and panel (B) shows a 3D reconstruction of the metathoracic tracheal tree in colors reflecting volumetric rendering, with the rest of the larval tracheal system in the segment semi-transparent. Panel (C) shows a volumetric rendering of a single metathoracic tracheal tree, with the spiracular opening in the bottom. Arrows point to some of the manually closed tracheae. Note that the posterior longitudinal trunks are obscured in the shown orientation. Panel (D) shows a network segmentation analysis of the same tree. These segmentation analyses were used to calculate the total length of tubing in trees, as well as the area of the respiratory surface. Arrows show the same as in (C). Air-filled structures are colored according to their local volumetric diameter and scaled as shown in panel (C). Anatomical orientation is shown in tripods, Z (blue) points in the lateral plane towards the left side, Y (green) towards the anterior end and X (red) towards the dorsal end. (For interpretation of the references to colour in this figure legend, the reader is referred to the web version of this article.)

take the shape of perfect cylinders of decreasing diameter. This latter area represents the surface area of the tracheal lumen, rather than the actual surface area of the trachea. This is likely greater due to the morphology of the trachea themselves, as the spiral architecture of the taenidia form a "micro-corrugated" epicuticular surface rather than a smooth one (Webster et al., 2015).

2.5. Statistical analyses

The 10-base logarithm of head capsule width was used in a linear regression analysis with body mass as covariate. The effect of μCT X-ray radiation on larval growth was investigated with a chi-square test where growth was scored as a gain in mass having occurred or not. For this analysis groups B and C were pooled. Repeatability of the segmentation methods were tested by performing the volumetric and length estimations on both the right and left individual tracheal tree within the same larva and then testing the correlation with a Pearsońs correlation test. Repeatability of the two methods of calculating tracheal tree area were also performed with a Pearsońs correlation test. Repeatability of tracheal trait measured between the two time-points was investigated with a paired-sample *t*-test. Separate linear regression analyses were performed for (i) resting metabolic rate, (ii) tracheal volume, (iii) tracheal tree length and, (iv) tracheal tree area. The 10-base logarithm of the traits were added as dependent variable, and the 10-base logarithm of body mass as continuous explanatory variable. In the current study there was not enough power to compare scaling coefficients in formal analyses, thus we simply investigated whether the traits scale with body mass or not and then visually compared slopes. The results for the scaling analyses are thus to be regarded as exploratory. The data were visually inspected for normality, while Whiteś test was used to ensure homoscedasticity of error variances. All statistical tests were performed using IBM SPSS statistics 25.0 (IBM SPSS Inc., Chicago, IL, USA).

3. Results

3.1. Growth and mortality during the rearing period

There was a strong and positive correlation between the width of the head capsule and the mass of the larva ($F_{1,12} = 92.578$, $P < 0.001$; Table 1). For this analysis, larval mass ranged from 1.4 g to 7.8 g, giving a fold change variation of 5.6 between the smallest and largest measured individual. Visual inspection of the size distribution shows three non-overlapping clusters of head capsule sizes, suggesting distinct groups, which we assume reflect the three last instars of development (Fig. 2A). Mass gain in larvae varied among the individuals, with some individuals increasing in mass, some remaining relatively unchanged, and some decreasing in mass (Fig. 2B). While this unexpectedly large variation in growth rates made investigating effects of radiation exposure challenging, the variation was equally large in the A and B + C groups ($\chi^2_{1, N=20} = 1.650$, $P = 0.199$). Out of the 8 individuals scanned twice, none died subsequent from the first scan before the second scanning event approximately 2 months later. The current study thus suggests that neither anesthesia using sevoflurane, nor the radiation dose absorbed during μCT scanning has a noticeable negative effect on survival or growth in *C. newmannii* larvae.

3.2. Comparison between two methods of calculating tracheal tree area

While the correlation between the two methods of calculating tracheal tree area was very high ($r_{N = 10} = 0.945$, $p < 0.001$), using VGSTUDIO MAX 3.2 provided an on average 2-fold higher area estimate than using Avizo Fire 9.5.0 (Fig. 3A). Since the former tracks uneven surfaces (down to the voxel size) the analysis shows that tracheal walls are more complex than the simplified open cylinders assumed by the latter method. While the methods differed in the area they provided, they produced comparable scaling relationships with body mass (data not shown), suggesting that the uneven surfaces exist across the full gradient of tracheal sizes. For the comparison of tracheal area against body mass (see below) we used the area determined through Avizo Fire 9.5.0.

3.3. Lateral comparison of tracheal trees

Correlation coefficients between the tracheal trees were high for both volume ($r_{N = 14} = 0.981$, $p < 0.001$) and total length ($r_{N = 14} = 0.958$, $p < 0.001$; Fig. 3B & 3C), indicating that the method used to estimate tracheal tree characteristics is highly repeatable. It also shows that the estimated traits of the tracheal trees are highly consistent anatomical features of an individual larva at a particular developmental stage.

3.4. Intra-individual growth in tracheal tree structures

Overall ranking of the tracheal tree traits was similar among the individuals at the two measurement time points and a paired sample *t*-test did not detect any overall significant change in tracheal tree volume ($t_{df = 7} = 0.017$, $P = 0.987$), length ($t_{df = 7} = 0.374$, $P = 0.719$) nor, area ($t_{df = 7} = 0.722$, $P = 0.494$). Roughly half of the individuals showed increases in the tracheal tree size, while the other half showed decreases (Fig. 4). One individual had a collapsed and fluid filled left tracheal tree, and showed a large decrease in all tracheal traits also in the right tree (marked red in Fig. 4).

3.5. Resting metabolic rate and tracheal tree structures vs body mass

Larvae in general showed discontinuous respiration during rest. Resting metabolic rate increased as a function of mass ($F_{1,33} = 23.677$, $P < 0.001$; Fig. 5A), with a coefficient of 1.086, thus suggesting scaling to be near isometric (Table 1). The volume ($F_{1,13} = 27.926$, $P < 0.001$),

Table 1
Coefficients for the regression analyses of the relationships between mass and the different traits investigated in the present study (head capsule width, resting metabolic rate and tracheal tree morphology) in larvae of the beetle *Cacosceles newmannii*.

Response	Factor	B	Std. Error	t	Sig.	LCI 95%	UCI 95%
log_head capsule (mm)	intercept	0.688	0.017	39.711	< 0.001	0.650	0.726
	log_mass	0.263	0.027	9.622	< 0.001	0.203	0.324
log_rmr (ml CO_2 h^{-1})	intercept	−1.257	0.100	−12.624	< 0.001	−1.459	−1.054
	log_mass	1.086	0.233	4.866	< 0.001	0.631	1.540
log_volume (mm^3)	intercept	−0.640	0.181	−3.544	0.004	−1.033	−0.246
	log_mass	1.511	0.286	5.285	< 0.001	0.888	2.134
log_length (μm)	intercept	1.474	0.140	10.516	< 0.001	1.169	1.779
	log_mass	1.018	0.222	4.588	0.001	0.535	1.502
log_area (mm^2)	intercept	0.720	0.176	4.091	0.001	0.337	1.104
	log_mass	1.208	0.279	4.332	0.001	0.601	1.816

LCI = lower confidence interval, and UCI = upper confidence interval.

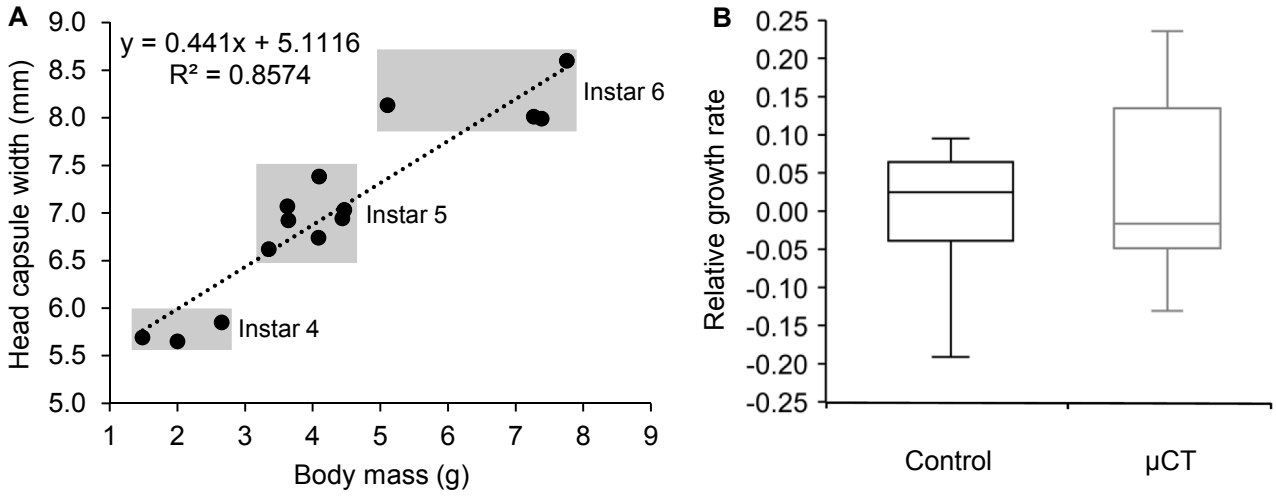

Fig. 2. In (A) the relationship between mass and head capsule width in individual *Cacosceles newmannii* larvae used in the present experiment. The grey boxes reflect the presumed three last instars of larval development (4–6). N = 14. Panel (B) shows the relative mass change between the first and second measurement round in control larvae and larvae exposed to µCT. A X^2 test suggested no difference between the groups (see results). N = 8 for µCT and N = 12 for control.

length ($F_{1,13} = 21.048$, P = 0.001) and, area ($F_{1,13} = 18.767$, P = 0.001) of tracheal trees also increased as functions of mass (Fig. 5B-D). The coefficients suggest hyperallometric scaling for tracheal volume (1.511) and area (1.208), and isometric scaling for tracheal length (1.018) (Table 1). Note however, that the sample size used in the present study is not sufficient to distinguish among major scaling coefficients (see large confidence intervals in Table 1) and should be viewed as exploratory, rather than definitive, results.

4. Discussion

A central challenge in studying insect respiratory structures and their variation is their microscopic size. While several methods for imaging insect respiratory systems are available, methods are generally lethal or destructive, time consuming or labour intensive (Harrison et al., 2018a; Iwan et al., 2015; Javal et al., 2019; Wasserthal et al., 2018). In the present study we therefore explore the possibility to use µCT based scanning to investigate tracheal growth in live insects. We were successfully able to sedate larvae (MacMillan et al., 2017), scan and reconstruct tracheal structures, and can show that exposure to the anesthetic and µCT radiation dose does not lead to increased mortality or a systematic difference in growth. Thus, we suggest the method presented here might be suitable for longitudinal studies on live, developing, insects (Lowe et al., 2013), to for instance track growth in tracheal traits as function of metabolic demand. This opens up new avenues to test morphology, performance and the potential fitness consequences, and thus obtain respiratory anatomical estimates as animals develop, grow and change shape in ways that have not been well explored in insects to date.

Here we aimed to develop the methodological proof of concept of live animal imaging, and further understanding of the potential methodological artifacts or limitations of our approach. The focus of this work was not primarily on developing robust scaling estimates for the slow-growing, large-bodied *C. newmannii* as this would require more systematic measurement across a far larger sample size to be more representative of the natural population, especially at the size extremes. Nevertheless, we report key scaling relationships as these may be useful in guiding future studies on these themes and some insights can be drawn based on the data at hand. The scaling relationship between body mass and metabolic demand (i.e. rmr) in larvae of *C. newmannii* was found to be near-isometric, with a scaling coefficient of 1.09 ± 0.23. While a meta-analysis of 391 insect species report a hypoallometric interspecific scaling coefficient of 0.82 (95% CI = 0.78 – 0.85), intraspecific relationships are broader and included near-isometric scaling coefficients (range 0.67 – 1.0) (Chown et al., 2007). Also other studies have reported isometric or near-isometric scaling in insects (e.g. Blossman-Myer and Burggren, 2010), and variation in scaling coefficients are often large, especially when including different life-stages (Glazier, 2005). Estimating the scaling relationship between resting metabolic rate and body mass in developing insects is non-trivial. Even though activity- and digestion-related metabolic rate can be controlled for (e.g. by starving individuals, and using activity detectors), development itself cannot, and will be a part of the compound trait that is resting metabolic rate (Glazier, 2005). In the current study this was part of the intended experimental design, since we were interested in determining how the scaling relationship of metabolic demand compared to the scaling relationship of metabolic supply as a function of development.

Unfortunately, development was more variable than anticipated, with some individuals increasing in mass, others decreasing in mass and most remaining relatively unchanged over the almost 60 day observation period. This high variability could be due to the wood-boring saproxylic nature of the larvae (i.e. living inside plant tissue), and reflects slow development reported for other beetle species with similar ecology (Gallardo and Cárdenas, 2016). The species was chosen for the current study due to its large size gradient (with some individuals reaching in excess of 12 g), but the large variation among individuals in growth rates suggests it is not perhaps an optimal model for the study of developmental physiology. While we therefore cannot make meaningful interpretation of within-instar developmental constraints (Helm and Davidowitz, 2013), we can investigate the relationship between metabolic demand and supply across the entire size range of our data – spanning at least three instars of development (Callier and Nijhout, 2011; Greenlee and Harrison, 2005).

The three tracheal traits determined here showed scaling relationships similar to that of rmr. Even though we did not directly compare scaling coefficients due to statistical power limitations, the data strongly suggest that the tracheal system does not scale hypoallometrically, and thus should not be rate-limiting in terms of providing oxygen to growing tissues in these beetle larvae. Instead, the data suggests hyperallometric (>1.00) scaling for tracheal tree volume and area and thus a potential excess capacity to deliver oxygen at larger sizes in this species. Similar scaling coefficients (1.16) between tracheal volume and body volume were observed in larvae of the beetle *Tenebrio molitor* (Raś et al., 2018). The hyperallometric relationship could be driven by an increasing aerobic scope with size since, at least in the locust *Locusta migratoria,* strong

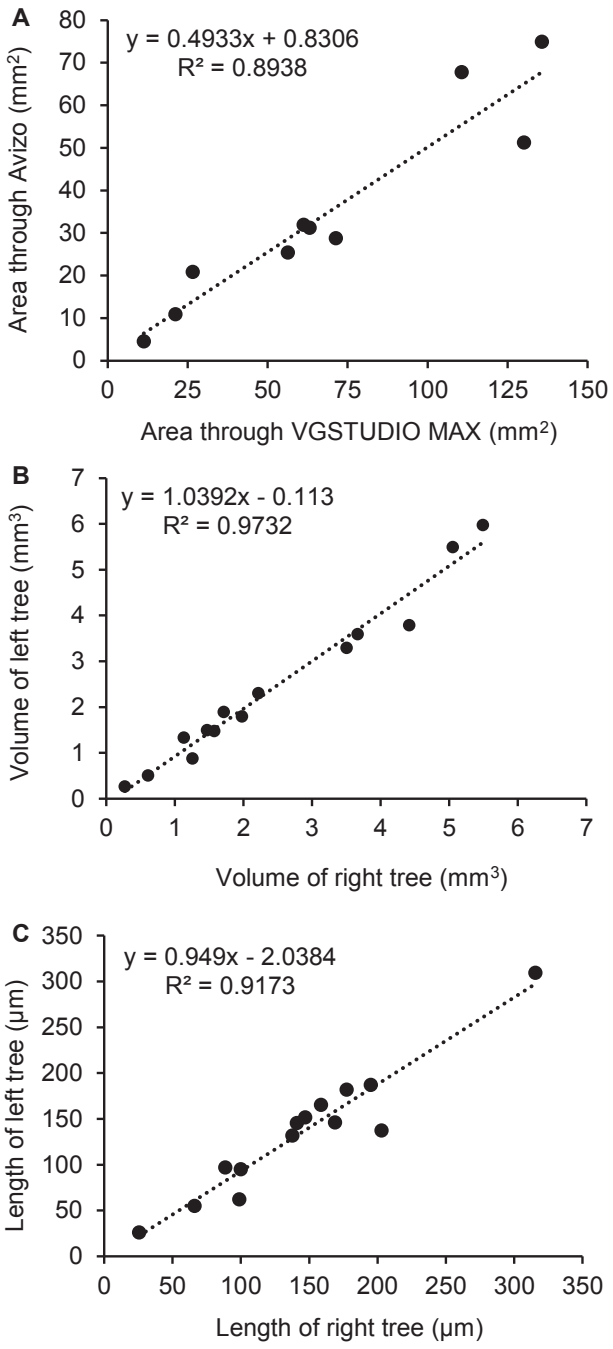

Fig. 3. Correlation between measures of tracheal trees in larvae of the beetle *Cacosceles newmannii*. Panel (A) shows tracheal tree area estimated using VGSTUDIO MAX 3.2 and Avizo Fire 9.5.0 respectively. Panel (B) shows total volume and panel (C) total length of the right and left first abdominal tracheal tree. In (A) N = 10, in (B) and (C) N = 14.

evidence for symmorphosis has been reported when investigating maximum metabolic rate (Snelling et al., 2011c). While we did not measure maximum metabolic rate or aerobic scope by exercise to exhaustion in the current study, aerobic scope was estimated in another study both for larvae and adults of *C. newmannii*, revealing a very narrow absolute aerobic scope of 1.68 ± 1.53 ml CO_2 h^{-1} in larvae compared to 5.97 ± 2.56 ml CO_2 h^{-1} in adults (Javal et al., 2019). A similarly narrow aerobic scope was determined in the same species using an independent data collection (Smit et al., 2021). The narrow aerobic scope could relate to the saproxylic nature of these larvae, and the absence of energy-demanding sustained activity levels in the larval life-stage. Therefore, while performing the measurements using maximum metabolic rate might have decreased the slope marginally, previous results suggest that a large aerobic scope should not be the cause for the apparent over-capacity of the oxygen supply system in these larvae (Javal et al., 2019).

One argument against an overcapacity of the tracheal system in delivering oxygen to the tissue is the so-called oxygen toxicity hypothesis (Hetz, 2007; Hetz and Bradley, 2005). As oxygen is toxic at high concentrations in animal cells, maintaining oxygen levels well above current demand should lead to the production of free oxygen radicals (Jamieson, 1989). These can be stressful on their own, but can also incur indirect costs in terms of mounting an antioxidant defense response (D'Autréaux and Toledano, 2007; Joanisse and Storey, 1996; Sanz et al., 2010). This should be especially true for species or life-stages with a limited aerobic scope, where the relative benefit of an oxygen-delivery overcapacity should be very small (but see Boardman et al., 2012). It is possible however that larvae of *C. newmannii* and other saproxylic species, are relatively protected by excess oxygen through chronic hypoxia in plant tissues (Spicer and Holbrook, 2005; Wittmann and Pfanz, 2014; Harrison et al., 2018b). Indeed, an overcapacity to take up and distribute oxygen might even be beneficial under such circumstances.

One important limitation in the current study was the achieved minimum resolution of 15 µm. Since the tracheal system consists of tubing with diameters decreasing down to less than 1 µm (Wigglesworth, 1983), a potentially large proportion of the tracheal system was not quantified. A study of adult *Hypothenemus hampei* beetles shows that the majority of tracheal volume resides in trachea with diameters of less than 10 µm and trachea with a diameter over 15 µm only represent less than 10% of total volume (Alba-Tercedor et al., 2019). This could primarily be due to the very small size of these beetles (adult body mass ~2 mg). Indeed, a study on the much larger bodied grasshopper *Schistocerca americana* (adult body mass >1 g) found a very strong correlation between different traditional methods of quantifying tracheal air volume and a µCT method using voxel sizes of 48 µm (Shaha et al., 2013), indicating that the 15 µm achieved in the present study might be sufficient for the large-bodied larvae used here.

Tracheal volume quantification using µCT are however further complicated by observations in *T. molitor* that varying voxel size (i.e. scan resolution) gives different results depending on the body compartment studied (Iwan et al., 2015; Raś et al., 2018). While using smaller voxel sizes increases total volume estimates on the whole body scale, a less steep relationship is seen if restricting the analysis to only the head and prothorax, probably due to differences in content of tissue with varying metabolic demand (Baccino-Calace et al., 2020; Weibel, 2002). Thus, when using hard cut-offs in tracheal diameter, it is difficult to know how much of total tracheal volume that actually is quantified, and how much is found in trachea and tracheoles with smaller diameters. Future studies could explore possibilities to improve minimum resolution, for instance using machine learning algorithms that improve capacity to distinguish tracheal structures in fuzzy images (Yang et al., 2020). More generally, it would be important to study insect species across a wide range of body sizes to determine the distribution of tracheal size relationships (Aitkenhead et al., 2020; Kaiser et al., 2007) at different scanning resolutions (Iwan et al., 2015).

The comparison between two methods of estimating tracheal surface generated strikingly different area estimates. The method based on Avizo Fire 9.5.0 assumed trachea take the shape of perfect cylinders of decreasing diameter, which likely is an oversimplification (Webster et al., 2015). This was indeed suggested by the more sensitive method using VGSTUDIO MAX 3.2, which generated an almost two-fold higher area estimate. This finding is significant, given that some metabolic studies indeed assume tracheal inner volume takes the form of a perfect cylinder of decreasing diameter (e.g. Grieshaber and Terblanche, 2015). Thus, we suggest further research and use of µCT in respiratory metabolism studies is warranted.

To conclude, we investigated the tracheal system in larvae of

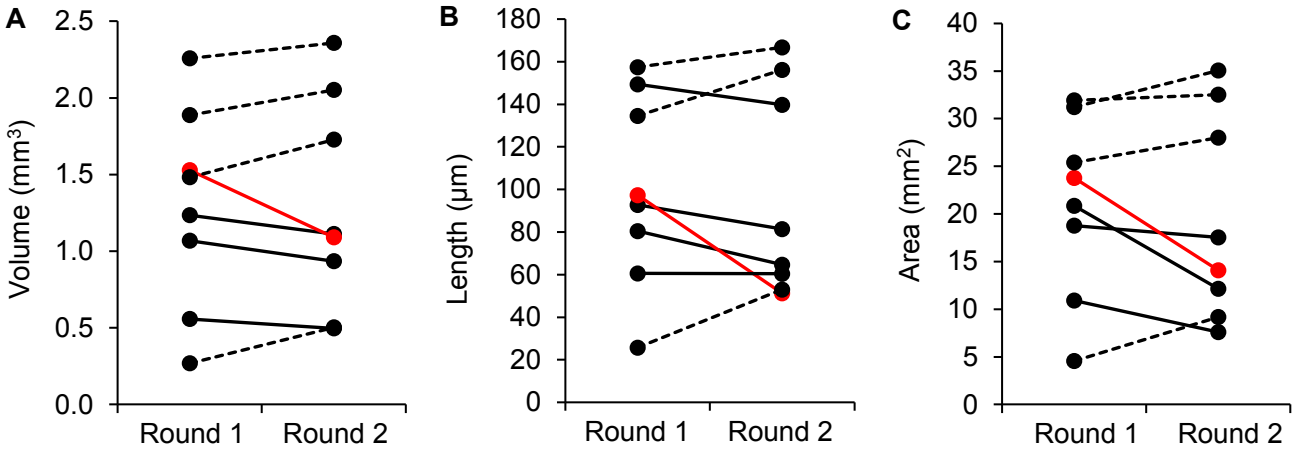

Fig. 4. Repeated measures of tracheal tree (A) volume, (B) length and (C) area in larvae of the beetle *Cacosceles newmannii*. Lines reflect change in trait where solid reflects negative and dashed positive growth. The red line reflects an individual with a collapsed left tracheal tree, and large decreases tracheal sizes of the right tree. N = 8. (For interpretation of the references to colour in this figure legend, the reader is referred to the web version of this article.)

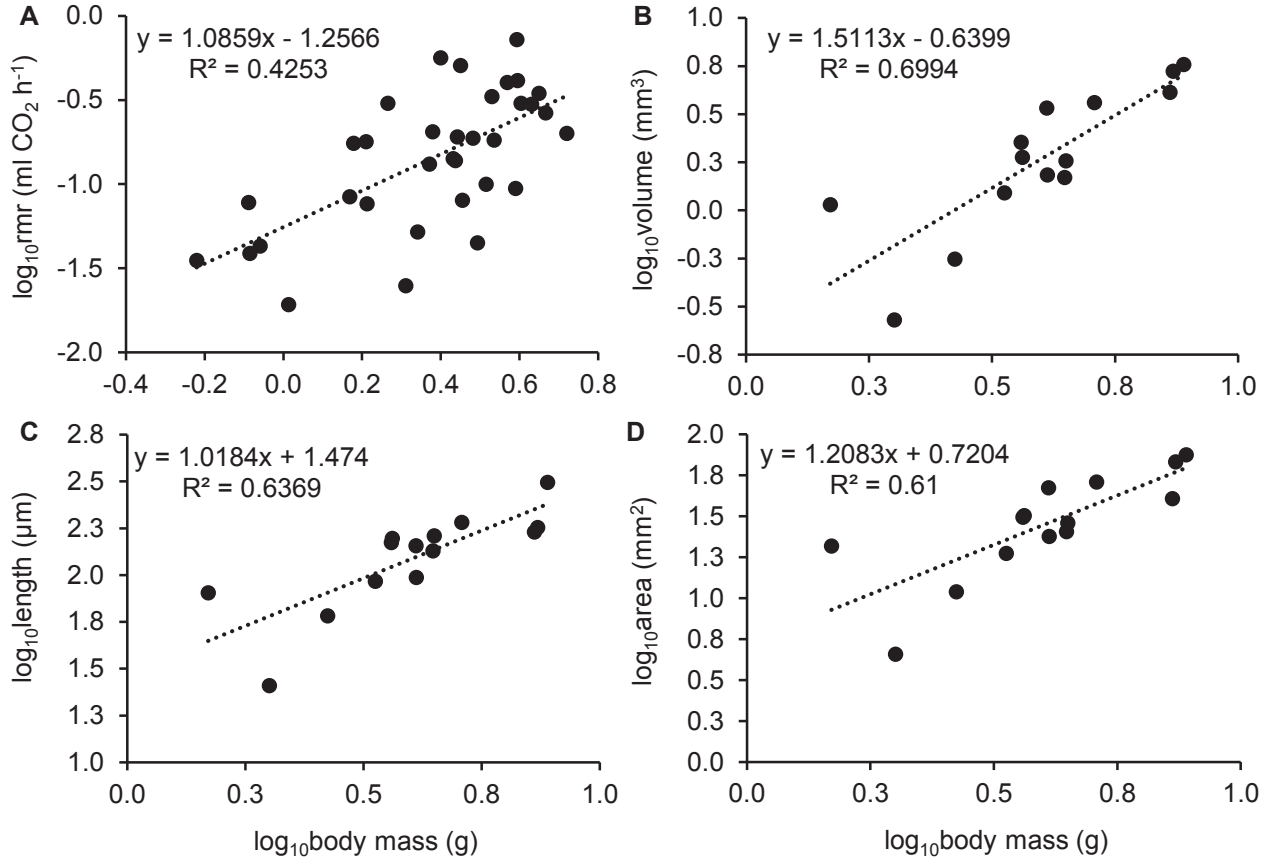

Fig. 5. Scaling relationships between mass and the four respiratory traits of interest in larvae of the beetle *Cacosceles newmannii*. Traits estimated are A) resting metabolic rate, B) tracheal tree volume, C) tracheal tree length and D) tracheal tree area. N = 34 in A and N = 14 in B-D.

C. newmannii, a large-bodied beetle with pronounced ontogenetic variation in mass. We were able to successfully sedate larvae and perform repeated measurements of tracheal traits down to a resolution of 15 µm on live individuals, opening up new methodological avenues for further study. It seems likely that using living organisms carries the cost of poorer resolution, which needs to be traded off against the benefit of having organs and internal structures in an anatomically appropriate configuration. While we were not able to investigate individual patterns of growth in metabolic demand (i.e. resting metabolic rate) and supply (i.e. tracheal dimensions), our preliminary analyses show evidence for matched growth of metabolic demand and oxygen supply over half an order of magnitude of mass gain in the larvae. In fact, the traits suggest overcapacity, rather than capacity deficit, at larger masses. While the results therefore suggest oxygen limitation is unlikely to be the cause for moulting in this species, they also raise the question as to why such an excess capacity is present. According to the theory of symmorphosis (Weibel et al., 1991), there should not be excess physiological capacity of a costly organ. Most likely therefore, the developmental program

regulating the growth and final size of the tracheal system is under multiple competing selection pressures (Kaiser et al., 2007; Callier and Nijhout, 2012) that over evolutionary time have shaped it into a well-functioning compromise between gas influx and efflux. In a recent study on tracheal scaling of ants, CO_2 efflux was determined to be the most important determinant of scaling patterns (Aitkenhead et al., 2020) and it would be of great interest to establish if this is a broader pattern occurring across the extremely large body size gradient present in the Insecta.

CRediT authorship contribution statement

Philipp Lehmann: Conceptualization, Methodology, Formal analysis, Writing - original draft, Visualization, Funding acquisition. **Marion Javal:** Methodology, Investigation, Data curation, Writing - review & editing. **Anton Du Plessis:** Visualization, Methodology, Validation, Investigation, Resources, Writing - review & editing. **John S. Terblanche:** Conceptualization, Writing - review & editing, Funding acquisition.

Acknowledgments

We are thankful for laboratory assistance from Chantelle Smit, and assistance with image segmentation from Stephan le Roux and Muofhe Tshibalanganda (CT scanner facility). The anonymous referees, Art Woods and Eva Ehrnsten are thanked for providing constructive comments on earlier versions of the manuscript. J.S.T. is grateful to Dr. Bryant Roux for assisting with the provision of sevoflurane. This work was supported by the Company of Biologists and Journal of Experimental Biology to P.L. (JEB-171103) and through a Center for Invasion Biology (CIB) Fellowship to P.L.

References

Aitkenhead, I.J., Duffy, G.A., Devendran, C., Kearney, M.R., Neild, A., Chown, S.L., 2020. Tracheal branching in ants is area-decreasing, violating a central assumption of network transport models. PLOS Comput. Biol. 16, e1007853 https://doi.org/10.1371/journal.pcbi.1007853.

Alba-Tercedor, J., Alba-Alejandre, I., Vega, F.E., 2019. Revealing the respiratory system of the coffee berry borer (*Hypothenemus hampei*; Coleoptera: Curculionidae: Scolytinae) using micro-computed tomography. Sci. Rep. 9, 17753. https://doi.org/10.1038/s41598-019-54157-3.

Baccino-Calace, M., Prieto, D., Cantera, R., Egger, B., 2020. Compartment and cell-type specific hypoxia responses in the developing *Drosophila* brain. Biol. Open 9, bio053629. https://doi.org/10.1242/bio.053629.

Blossman-Myer, B.L., Burggren, W.W., 2010. Metabolic allometry during development and metamorphosis of the Silkworm *Bombyx mori* : Analyses, patterns, and mechanisms. Physiol. Biochem. Zool. 83, 215–231. https://doi.org/10.1086/648393.

Boardman, L., Terblanche, J.S., 2015. Oxygen safety margins set thermal limits in an insect model system. J. Exp. Biol. 218, 1677–1685.

Boardman, L., Terblanche, J.S., Hetz, S.K., Marais, E., Chown, S.L., 2012. Reactive oxygen species production and discontinuous gas exchange in insects. Proc. R. Soc. B Biol. Sci. 279, 893–901. https://doi.org/10.1098/rspb.2011.1243.

Callier, V., Nijhout, H.F., 2012. Supply-side constraints are insufficient to explain the ontogenetic scaling of metabolic rate in the tobacco hornworm, *Manduca sexta*. PLoS ONE 7, e45455. https://doi.org/10.1371/journal.pone.0045455.

Callier, V., Nijhout, H.F., 2011. Control of body size by oxygen supply reveals size-dependent and size-independent mechanisms of molting and metamorphosis. Proc. Natl. Acad. Sci. U.S.A. 108, 14664–14669.

Chapman, R.F., 2012. The Insects – Structure and Function, 5th ed. Cambridge University Press.

Chown, S.L., Marais, E., Terblanche, J.S., Klok, C.J., Lighton, J.R.B., Blackburn, T.M., 2007. Scaling of insect metabolic rate is inconsistent with the nutrient supply network model. Funct. Ecol. 21, 282–290. https://doi.org/10.1111/j.1365-2435.2007.01245.x.

D'Autréaux, B., Toledano, M.B., 2007. ROS as signalling molecules: mechanisms that generate specificity in ROS homeostasis. Nat. Rev. Mol. Cell Biol. 8, 813–824. https://doi.org/10.1038/nrm2256.

du Plessis, A., Broeckhoven, C., Guelpa, A., le Roux, S.G., 2017. Laboratory x-ray micro-computed tomography: a user guideline for biological samples. GigaScience 6, 1–11.

Ferreira, G.W.S., 1980. The Parandrinae and the Prioninae of southern Africa (Cerambycidae, Coleoptera), Memoirs van die Nasionale Museum ;nr. 13. Nasionale Museum, Bloemfontein, Republiek van Suid-Afrika.

Gallardo, P., Cárdenas, A.M., 2016. Long-term monitoring of saproxylic beetles from Mediterranean oak forests: An approach to the larval biology of the most representative species. J. Insect Conserv. 20, 999–1009. https://doi.org/10.1007/s10841-016-9934-2.

Glazier, D.S., 2005. Beyond the '3/4-power law': Variation in the intra- and interspecific scaling of metabolic rate in animals. Biol. Rev. 80, 611. https://doi.org/10.1017/S1464793105006834.

Greenlee, K.J., Harrison, J.F., 2005. Respiratory changes throughout ontogeny in the tobacco hornworm caterpillar, *Manduca sexta*. J. Exp. Biol. 208, 1385–1392.

Greenlee, K.J., Henry, J.R., Kirkton, S.D., Westneat, M.W., Fezzaa, K., Lee, W.-K., Harrison, J.F., 2009. Synchrotron imaging of the grasshopper tracheal system: morphological and physiological components of tracheal hypermetry. Am. J. Physiol.-Regul. Integr. Comp. Physiol. 297, R1343–R1350. https://doi.org/10.1152/ajpregu.00231.2009.

Grieshaber, B.J., Terblanche, J.S., 2015. A computational model of insect discontinuous gas exchange: a two-sensor, control systems approach. J. Theor. Biol. 374, 138–151. https://doi.org/10.1016/j.jtbi.2015.03.030.

Harrison, J.F., Greenlee, K.J., Verberk, W.C.E.P., 2018a. Functional hypoxia in insects: definition, assessment, and consequences for physiology, ecology, and evolution. Annu. Rev. Entomol. 63, 303–325. https://doi.org/10.1146/annurev-ento-020117-043145.

Harrison, J.F., Waters, J.S., Biddulph, T.A., Kovacevic, A., Klok, C.J., Socha, J.J., 2018b. Developmental plasticity and stability in the tracheal networks supplying Drosophila flight muscle in response to rearing oxygen level. J. Insect Physiol. 106, 189–198. https://doi.org/10.1016/j.jinsphys.2017.09.006.

Harrison, J.F., Woods, H.A., Roberts, S.P., 2012. Ecological and Environmental Physiology of Insects. Oxford University Press, United Kingdom.

Helm, B.R., Davidowitz, G., 2013. Mass and volume growth of an insect tracheal system within a single instar. J. Exp. Biol. 216, 4703–4711.

Hetz, S.K., 2007. The role of the spiracles in gas exchange during development of *Samia cynthia* (Lepidoptera, Saturniidae). Comp. Biochem. Physiol. Mol. Integr. Physiol. 148, 743–754.

Hetz, S.K., Bradley, T.J., 2005. Insects breathe discontinuously to avoid oxygen toxicity. Nature 433, 516–519.

Iwan, D., Kamiński, M.J., Raś, M., 2015. The last breath: A μCT-based method for investigating the tracheal system in Hexapoda. Arthropod Struct. Dev. 44, 218–227. https://doi.org/10.1016/j.asd.2015.02.002.

Jamieson, D., 1989. Oxygen toxicity and reactive oxygen metabolites in mammals. Free Radic. Biol. Med. 7, 87–108. https://doi.org/10.1016/0891-5849(89)90103-2.

Javal, M., Thomas, S., Lehmann, P., Barton, M.G., Conlong, D.E., Du Plessis, A., Terblanche, J.S., 2019. The effect of oxygen limitation on a xylophagous insect's heat tolerance is influenced by life-stage through variation in aerobic scope and respiratory anatomy. Front. Physiol. 10, 1426. https://doi.org/10.3389/fphys.2019.01426.

Joanisse, D.R., Storey, K.B., 1996. Oxidative stress and antioxidants in overwintering larvae of cold-hardy goldenrod gall insects. J. Exp. Biol. 199, 1483–1491.

Kaiser, A., Klok, C.J., Socha, J.J., Lee, W.-K., Quinlan, M.C., Harrison, J.F., 2007. Increase in tracheal investment with beetle size supports hypothesis of oxygen limitation on insect gigantism. Proc. Natl. Acad. Sci. 104, 13198–13203. https://doi.org/10.1073/pnas.0611544104.

Kivelä, S., Lehmann, P., Gotthard, K., 2016. Does oxygen supply constrain metabolism of larval insects before moulting: an empirical test at the individual level. J. Exp. Biol. 219, 3061–3071.

Lowe, T., Garwood, R.J., Simonsen, T.J., Bradley, R.S., Withers, P.J., 2013. Metamorphosis revealed: time-lapse three-dimensional imaging inside a living chrysalis. J. R. Soc. Interface 10, 20130304.

MacMillan, H.A., Nørgård, M., MacLean, H.J., Overgaard, J., Williams, C.J.A., 2017. A critical test of *Drosophila anaesthetics*: Isoflurane and sevoflurane are benign alternatives to cold and CO2. J. Insect Physiol. 101, 97–106.

Matthews, P.G.D., Snelling, E.P., Seymour, R.S., White, C.R., 2012. A test of the oxidative damage hypothesis for discontinuous gas exchange in the locust *Locusta migratoria*. Biol. Lett. 8, 682–684.

Miller, P.L., 1966. The supply of oxygen to the active flight muscles of some large beetles. J. Exp. Biol. 45, 285–304.

Niven, J.E., Laughlin, S.B., 2008. Energy limitation as a selective pressure on the evolution of sensory systems. J. Exp. Biol. 211, 1792–1804.

Raś, M., Iwan, D., Kamiński, M.J., 2018. The tracheal system in post-embryonic development of holometabolous insects: a case study using the mealworm beetle. J. Anat. 232, 997–1015.

Sanz, A., Stefanatos, R., McIlroy, G., 2010. Production of reactive oxygen species by the mitochondrial electron transport chain in *Drosophila melanogaster*. J. Bioenerg. Biomembr. 42, 135–142. https://doi.org/10.1007/s10863-010-9281-z.

Schmitz, A., Perry, S.F., 1999. Stereological determination of tracheal volume and diffusing capacity of the tracheal walls in the stick insect *Carausius morosus* (Phasmatodea, Lonchodidae). Physiol. Biochem. Zool. 72, 205–218. https://doi.org/10.1086/316655.

Shaha, R.K., Vogt, J.R., Han, C.-S., Dillon, M.E., 2013. A micro-CT approach for determination of insect respiratory volume. Arthropod Struct. Dev. 42, 437–442. https://doi.org/10.1016/j.asd.2013.06.003.

Smit, C., Javal, M., Lehmann, P., Terblanche, J.S., 2021. Metabolic responses to starvation and feeding contribute to the invasiveness of an emerging pest insect. J. Insect Physiol. 128, 104162 https://doi.org/10.1016/j.jinsphys.2020.104162.

Snelling, E.P., Seymour, R.S., Matthews, P.G.D., Runciman, S., White, C.R., 2011a. Scaling of resting and maximum hopping metabolic rate throughout the life cycle of the locust *Locusta migratoria*. J. Exp. Biol. 214, 3218–3224.

Snelling, E.P., Seymour, R.S., Runciman, S., 2011b. Moulting of insect tracheae captured by light and electron-microscopy in the metathoracic femur of a third instar locust *Locusta migratoria*. J. Insect Physiol. 57, 1312–1316.

Snelling, E.P., Seymour, R.S., Runciman, S., Matthews, P.G.D., White, C.R., 2011c. Symmorphosis and the insect respiratory system: Allometric variation. J. Exp. Biol. 214, 3225–3237.

Spicer, R., Holbrook, N.M., 2005. Within-stem oxygen concentration and sap flow in four temperate tree species: does long-lived xylem parenchyma experience hypoxia? Plant Cell Environ. 28, 192–201. https://doi.org/10.1111/j.1365-3040.2004.01262.x.

Wasserthal, L.T., Cloetens, P., Fink, R.H., Wasserthal, L.K., 2018. X-ray computed tomography study of the flight-adapted tracheal system in the blowfly *Calliphora vicina*, analysing the ventilation mechanism and flow-directing valves. J. Exp. Biol. 221, jeb176024. https://doi.org/10.1242/jeb.176024.

Webster, M.R., Socha, J.J., Teresi, L., Nardinocchi, P., De Vita, R., 2015. Structure of tracheae and the functional implications for collapse in the American cockroach. Bioinspir. Biomim. 10, 066011 https://doi.org/10.1088/1748-3190/10/6/066011.

Weibel, E.R., 2002. The pitfalls of power laws. Nature 417, 131–132. https://doi.org/10.1038/417131a.

Weibel, E.R., Taylor, C.R., Hoppeler, H., 1991. The concept of symmorphosis: a testable hypothesis of structure-function relationship. Proc. Natl. Acad. Sci. U.S.A. 88, 10357–10361.

Wigglesworth, V.B., 1983. The physiology of insect tracheoles. Adv. Insect Physiol. 17, 85–148.

Wigglesworth, V.B., 1954. Growth and regeneration in the tracheal system of an insect, *Rhodnius prolixus* (Hemiptera). Q. J. Microsc. Sci. 95, 115–137.

Wigglesworth, V.B., 1930. A theory of tracheal respiration in insects. Proc. R. Soc. B 591, 229–250.

Wittmann, C., Pfanz, H., 2014. Bark and woody tissue photosynthesis: a means to avoid hypoxia or anoxia in developing stem tissues. Funct. Plant Biol. 41, 940. https://doi.org/10.1071/FP14046.

Yang, H., Su, X., Chen, S., Zhu, W., Ju, C., 2020. Efficient learning-based blur removal method based on sparse optimization for image restoration. PLOS ONE 15, e0230619. https://doi.org/10.1371/journal.pone.0230619.